26. NATURE, CHEMISTRY, AND ORIGIN OF LATE CENOZOIC MEGASCOPIC TEPHRAS IN LEG 90 CORES FROM THE SOUTHWEST PACIFIC[1]

Campbell S. Nelson, University of Waikato
and
Paul C. Froggatt and Gregory J. Gosson, Victoria University[2]

ABSTRACT

Several thin (1–10 cm) megascopic vitric tephras occur in the late Cenozoic calcareous oozes on Lord Howe Rise in the Tasman Sea and off eastern South Island, New Zealand. Of the 18 tephras analyzed 15 are silicic (75–78% SiO_2) with abundant clear glass shards and a biotite ± hypersthene ± green hornblende ferromagnesian mineralogy. The Neogene silicic tephras were derived from the now-extinct Coromandel volcanic area in New Zealand, and the Quaternary ones from the presently active Central Volcanic Region of New Zealand. On the basis of glass chemistry and age, several of the Quaternary tephras are probably correlatives, and at least two can be matched to the major on-land Mt. Curl tephra (~0.25 m.y.). The occurrence of correlative silicic tephras both northwest and southeast of New Zealand may result from particularly violent eruptions, the ash below and above an altitude of ~20 km being dispersed in opposite directions toward the Pacific Ocean and Tasman Sea, respectively. Ash drifting eastward into the southeasterly trade wind belt off northeastern New Zealand could also be carried into the central and northern Tasman Sea.

Three megascopic tephras consist of altered basic shards and common labradorite crystals. They record Neogene explosive basaltic to andesitic activity from nearby ocean island or ridge sources in the Ontong-Java Plateau and Vanuatu regions.

The megascopic tephras are a very incomplete and biased record of late Cenozoic explosive volcanism in the southwest Pacific because the innumerable, thin, green argillaceous layers in the cores (Gardner et al., this volume) probably represent devitrified intermediate to basic tephras derived mainly from oceanic arc volcanism along the Pacific/Australia plate boundary. In contrast to the New Zealand–derived silicic glass shards, the preservation potential of these more basic shards in Leg 90 calcareous sediments was low.

INTRODUCTION

The southwest Pacific region has been characterized by extensive volcanism throughout the late Cenozoic (Fig. 1). Volcanic ash deposited in deep-sea sediments accumulating in the vicinity and downwind of eruptive centers can provide an accurate record of explosive volcanic activity (Kennett, 1981). In turn, the tephras form invaluable stratigraphic marker horizons with the potential for dating the associated sediments and correlating them over considerable distances.

Leg 90 drilling obtained high-quality cores through middle to late Cenozoic sediments at nine sites (586–594) in the southwest Pacific (Fig. 1). All sites were located in water depths of between 1000 and 2200 m, principally on the Lord Howe Rise in Tasman Sea, but also on the Ontong-Java Plateau in the western Pacific and off eastern South Island, New Zealand. The cores consist dominantly of foraminifer-bearing nannofossil oozes and chalks, with few and minor unconformities in their Neogene-Quaternary part. Hemipelagic oozes occur at the southernmost site (Site 594) close to New Zealand. The sediments were drilled using the hydraulic piston corer and extended core barrel systems (see Introductory chapter, this volume). These provided not only high core recovery (average 90%), but also excellent sections that are much less disturbed than the rotary cores previously obtained from the region on DSDP Legs 21 and 29 (Burns, Andrews, et al., 1973; Kennett, Houtz, et al., 1975). Conditions were optimal for detecting discrete tephra layers and other minor lithologies within the soft oozes. In anticipation of this, one of the precruise objectives of Leg 90 was the development of a deep-sea tephrostratigraphy for the region (see Introductory chapter, this volume).

Only a relative small number of visible vitric tephra layers were detected during core description (Appendix). However, trace amounts (<1%) of colorless and occasional brown glass shards were ubiquitous sediment components; their occurrence as revealed in routine shipboard smear slides has been summarized for five sites by Gardner, Nelson, et al. (this volume). Conceivably, careful processing of channel samples from cores may ultimately provide a useful tephrostratigraphy based on this finely dispersed volcanic glass fraction (e.g., Watkins and Huang, 1977). On the other hand, Gardner, Nelson, et al. (this volume) have suggested that diagenetic processes played a major role in determining and possibly masking the distribution of volcanic material in the Tasman Sea sites. They inferred that a proportion of the glassy component may have been dissolved from those sediments in contact with silica-undersaturated Antarctic Intermediate Water on Lord Howe Rise and, moreover, that common pale green laminae in the nannofossil oozes and chalks may represent the smectitized alteration products of former thin ash layers.

---

[1] Kennett, J. P., von der Borch, C. C., et al., *Init. Repts. DSDP*, 90: Washington (U.S. Govt. Printing Office).

[2] Addresses:(Nelson) Department of Earth Sciences, University of Waikato, Hamilton, New Zealand; (Froggatt) Centre for Continuing Education and Department of Geology, Victoria University, Wellington, New Zealand; (Gosson) Department of Geology, Victoria University, Wellington, New Zealand.

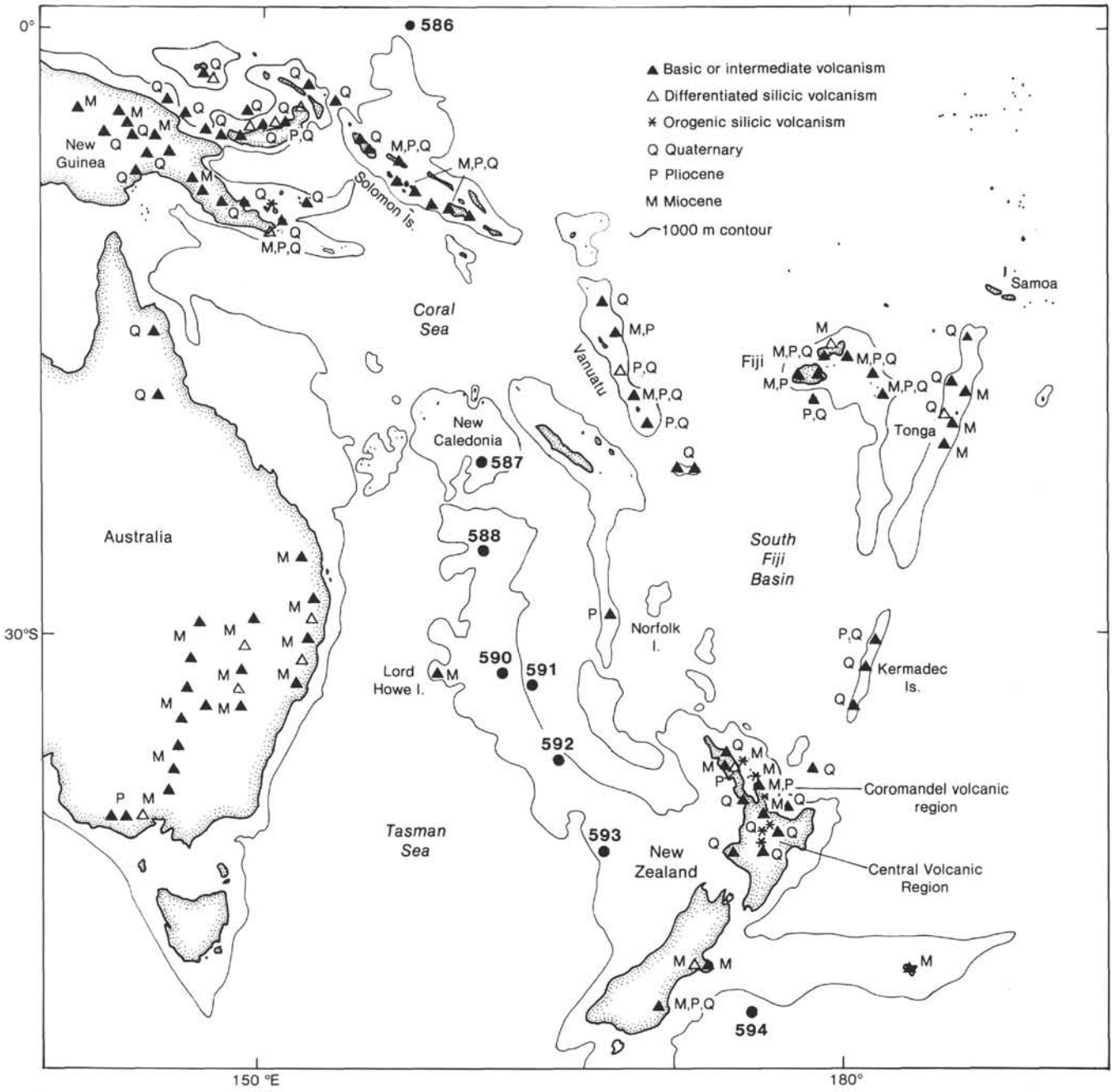

Figure 1. Distribution and character of Neogene and Quaternary subaerial volcanism in the southwest Pacific region (modified from Churkin and Packham, 1973; after Gosson, in prep.) in relation to DSDP Leg 90 Sites 586 to 594.

This chapter describes only those glass-dominated ash layers forming discrete, megascopic layers (= tephras) in Leg 90 cores. The principal objectives are to note the mineralogy of the tephras; determine the chemical composition of their glass shards, and hence the nature of the magmas; investigate the possibility of intercore tephra correlations; and suggest possible eruptive sources for the tephras.

RECOGNITION AND COLLECTION OF MEGASCOPIC TEPHRAS

During routine shipboard description of Leg 90 cores, special attention was paid to the occasional minor lithologies encountered within the lithologically monotonous sequences of calcareous oozes and chalks. The majority of these minor lithologies were pale green (bentonitic) laminae (Gardner, Nelson, et al., this volume); sediment layers enriched in pyrite, biosiliceous material, or glauconite; and diagenetic color-enhanced bioturbation structures (Nelson, this volume). The minor lithologies occasionally contained conspicuous glass shards, suggesting they represented primary air-fall tephra that had settled through the water column to the sea bed. In these cases, 5–10 cm^3 samples of the ash material plus contaminating host ooze were collected by the sedimentologists on duty. On shore, the summary core and smear

slide descriptions were perused again and additional, supposedly glass-rich, samples were requested to fill in some of the gaps in the collection of megascopic ash samples. A total of 54 samples was examined finally, but only 18 (T1 to T18) contained sufficiently abundant glass undisputedly to represent discrete tephra layers (see Appendix).

ANALYTIC METHODS

To determine the tephra sand mineralogy, samples were wet-sieved through a 63-μm mesh sieve, cleaned in an ultrasonic bath, wet-sieved again to remove impurities, and dried at 70°C. At this stage samples consisted of glass shards, varying amounts of foraminiferal tests, and small quantities of felsic, mafic, and opaque minerals. After first being checked for magnetite with a hand magnet, these components were separated by repeated passage of the sample through a Frantz Isodynamic electromagnetic separator (20° forward and 15° side slope). The majority of mafic and felsic minerals (other than pyrite) was contained in the magnetic fraction at 0.5–0.8 A, whereas glass and foraminifer grains were concentrated in the magnetic and nonmagnetic fractions, respectively, at 1.8 A. Any foraminifers remaining in the glass shard extract at this stage were removed. Minerals were identified in detrital slide mounts using a petrographic microscope, and the glass shards were examined both in thin section and with a scanning electron microscope.

The chemical composition of glass shards from 16 of the 18 megascopic tephras has been determined using an electron microprobe. A beam of 8 nA and 20 μm diameter was used to minimize alkali loss. Instrumental conditions and standard analyses are in Froggatt (1983). All of the analyzed shards were visually isotropic and free of microlites and inclusions. Homogeneity of each sample was checked by analyzing freshly polished internal surfaces of 12 to 15 shards. All glass analyses are recalculated to 100%, the deficiency being recorded as H_2O. This water is presumed to be gained by postdepositional hydration and values are typical of silicic tephras (see Froggatt, 1983). Tephras T2 and T3 contained too few unaltered shards for analysis, but the chemical composition of the plagioclase crystals in T3 (and also T1) has been determined.

DISTRIBUTION, APPEARANCE, AND AGE OF TEPHRAS

The stratigraphic locations of the 18 megascopic tephras studied are shown in Figure 2 and their appearance in cores in Figure 3. Samples, stratigraphy, and descriptive information for the individual tephras are summarized in Table 1.

Compared to the white (N9) to very light gray (N8) color of the host calcareous oozes (chalks), the tephras have distinctly greenish hues, ranging from light to dark greenish gray. They are typically only a centimeter or two thick, occasionally reaching 10 cm and exceptionally (T5) 25 cm. Several have sharp lower contacts, some exhibit normal size grading, and most have diffuse upper contacts with evidence of upward dissemination of ash by bioturbation into the overlying ooze (Fig. 3). Bioturbate structures are discernible within the thicker tephras, and biogenic reworking has totally disrupted some of the thinner ash layers and concentrated ash material as diffuse wisps, blebs, and pods within the host ooze.

Ten of the tephras are of Quaternary age, three are Pliocene, and five are Miocene (Fig. 2). Biostratigraphic age estimates are shown in Table 1. Absolute ages have been estimated by assuming a constant rate of sedimentation between an ash layer and the nearest paleomagnetic chron or subchron boundary in the case of each of the Quaternary tephras, and the nearest calcareous nannoplankton zone boundary for each of the Tertiary tephras (see Site chapters, this volume). In several cases two

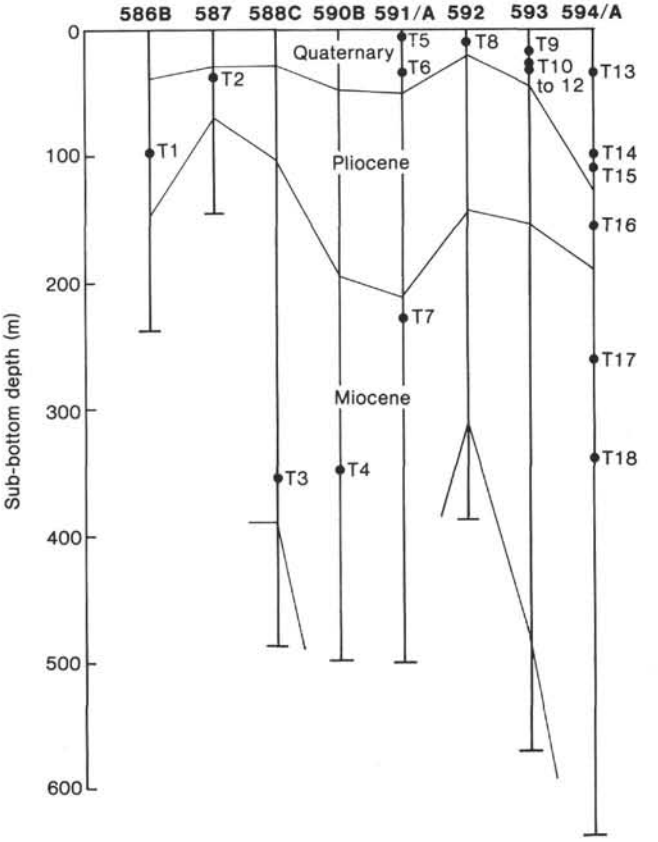

Figure 2. Stratigraphic distribution of the analyzed 18 megascopic tephras (T1 to T18) from Leg 90 sediments.

separate ages have been estimated, one using paleomagnetic and the other biostratigraphic information, or by employing datums both above and below an ash layer. In those cases the preferred age estimate of the tephra is italicized in Table 1.

PETROGRAPHY OF TEPHRAS

Because many of the sampled tephras included host calcareous ooze material, it was not possible to determine detailed textural properties for the discrete tephra layers. However, all were noticeably coarser than the associated oozes, and most had very fine to fine sandy textures (Table 2). The coarsest ash material occurred in samples (T1 to T3) from the three northernmost sites.

The sand fraction mineralogy of the 18 megascopic tephras is summarized in Table 2. Except for tephra T3, they are dominated by clear and/or milky glass shards (Plate 1). The minor crystalline components consist mainly of plagioclase, biotite, hypersthene, and green hornblende. White to pale green smectite-dominated aggregates occur in several samples and have formed possibly from the alteration of former glass or glassy rock fragments (cf. Gardner, Nelson, et al., this volume). Other alteration products include limonitized and leucoxene-coated (?) grains. In tephra T2 the glass is mostly devitrified but retains its shard morphology; in tephra T3 no free glass shards remain and the ash consists principally of feldspars, some with remnant glass jackets, and clay aggregates. Diagenetic pyrite (Table 3) occurs in some

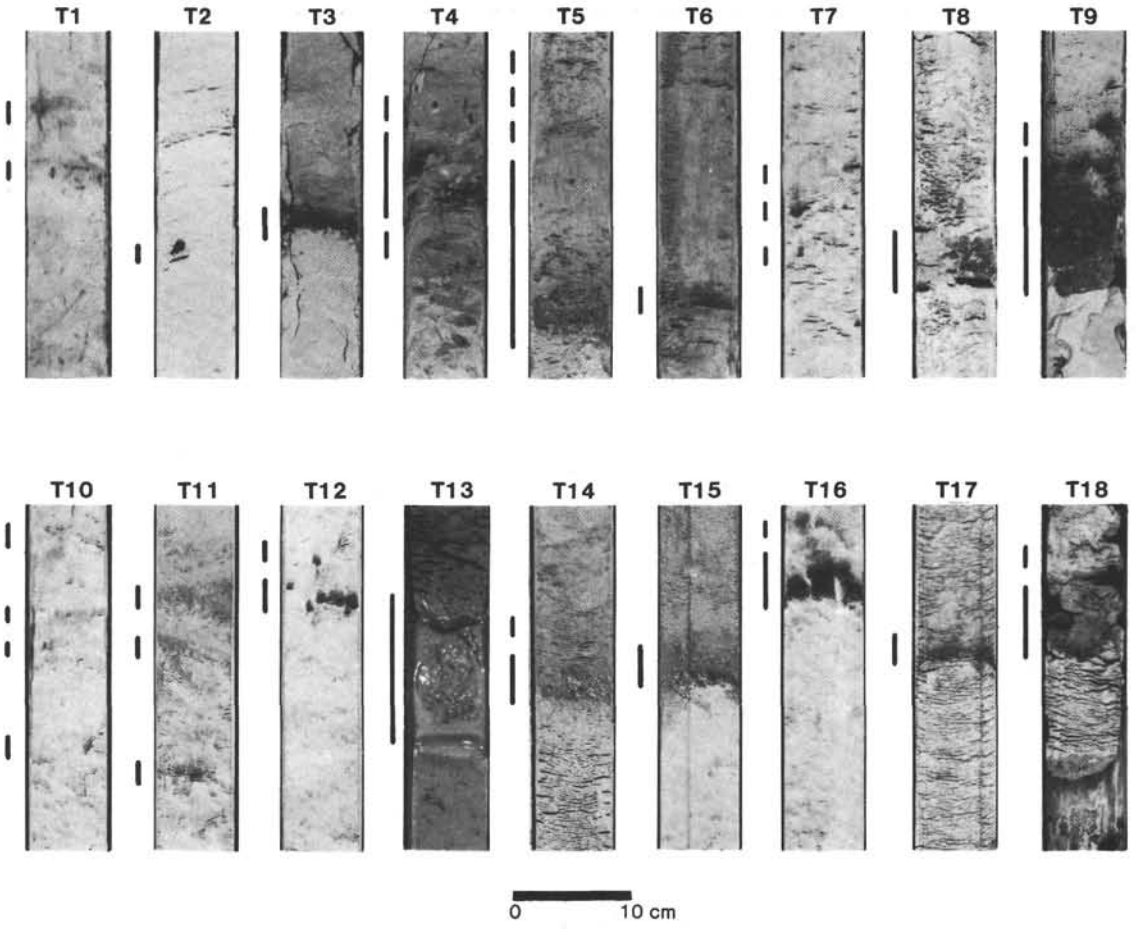

Figure 3. Appearance of the 18 megascopic tephras (T1 to T18) in Leg 90 cores (see Table 1 for descriptions of individual tephras). The bar to the left of each 30-cm-long core section indicates the position of the tephras. Core sections are located as follows: T1, 586B-11-3, 100–130 cm; T2, 587-5-5, 30–60 cm; T3, 588C-6-3, 35–65 cm; T4, 590B-38-4, 100–130 cm; T5, 591-2-2, 30–60 cm; T6, 591-5-3, 120–150 cm; T7, 591A-25-3, 10–40 cm; T8, 592-2-6, 65–95 cm; T9, 593-3-5, 65–95 cm; T10, 593-4-4, 20–50 cm; T11, 593-4-4, 60–90 cm; T12, 593-4-4, 90–120 cm; T13, 594-5-2, 20–50 cm; T14, 594-12-2, 25–55 cm; T15, 594A-8-3, 35–65 cm; T16, 594A-10-6, 0–30 cm; T17, 594-28-5, 45–75 cm; T18, 594-36,CC (0–30 cm).

samples. It forms a coating on glass shards in tephra T1 (Plate 1, Fig. 1; Fig. 4A) and is a microcrystalline replacement of the glass in tephra T4 (Fig. 4B), forming completely pyritized shards in some.

A scheme (Fig. 5) developed by G. J. Gosson (in prep.) is used here to classify the dominant glass shard morphologies in the 60–250 μm size range of the megascopic tephras (Table 4). The bulk of the Leg 90 shards are only slightly stretched with relatively few vesicles, and bubbles are moderately large with moderately thick walls (Tables 4). As a consequence, many of the shards form subequant- to rectangular-shaped, flat to gently curved plates, with up to two or three low-amplitude parallel ridges in some. Tephras T1 and T2 are distinctive because they are highly vesicular with relatively small bubble sizes and thin walls. A small percentage of shards in tephras T7, T8, T14, T15, and T17 are very stretched and highly vesicular. A feature of Miocene samples T17 and T18 is the polygonal shape of some bubble walls.

TEPHRA CHEMISTRY AND MAGMA TYPES

The glass analyses (Table 5) indicate that tephras T4 to T18 are all silicic (SiO_2 from 73.7 to 78.3 wt. % on an anhydrous basis) with broadly similar chemistry but varying amounts of most elements, especially the alkalis and iron and calcium. The variation in glass chemistry is evident on a plot of CaO versus FeO (Fig. 6) where, apart from tephra T15 (= 0 on Fig. 6), the glass analyses from individual tephras are relatively tightly clustered and many are unique. The occurrence of biotite, hypersthene, and/or green hornblende in the majority of these tephras (Table 2) is also consistent with a silicic volcanic source (Ewart, 1966; Kohn, 1973; Ewart et al., 1975; Seward, 1976; Cole, 1979). In contrast, tephra T1 is basaltic and has K_2O, TiO_2, SiO_2, and MgO values typical of ocean island or a more evolved mid-ocean ridge basalt (Table 6). Normative mineralogy of tephra T1 glass composition indicates it is quartz tholeiite, and the feldspar is calcic-labradorite (Table 7). Despite the lack of suitable glass for analysis in samples T2 and T3, both probably are basic also because (1) the abundant plagioclase crystals in T3 are sodic-labradorite (Table 7); (2) the devitrified glass shard morphologies in T2 are very similar to those in T1 (Table 4), and, in particular, both have very thin bubble walls suggestive of a low-viscosity magma; and (3) all three tephras (T1 to T3) lack the ferromagnesian

Table 1. Stratigraphy of megascopic vitric tephras in Leg 90 cores.

Tephra	Site	Core-Section (interval in cm)	Sub-bottom depth (m)	Thickness (cm)	Age		Lithologic description
					Period	m.y.[a]	
T1	586	11B-3, 114	100.44	<1	early Plio.	3.87[1]	Diffuse light greenish gray (5G 8/1) ash pods formed by bioturbation
T2	587	5-5, 48	38.28	<1	early Plio.	2.91[2] *3.70*[1]	Distinct dark gray (N3) ash pod formed by bioturbation
T3	588	6C-3, 52	357.25	2	early Mio.	22.0[1]	Distinct dark bluish gray (5BG 4/1) ash layer, sharp base, burrowed diffuse top
T4	590	38B-4, 113	351.15	10	late Mio.	11.0[1]	Prominently bioturbated, disrupted dark greenish gray (5GY 4/1) ash bed, pyritiferous, associated PGLs[b]
T5	591	2-2, 54	5.45	25	late Pleist.	0.24[2]	Diffuse light gray to light greenish gray (N7 to 5G 8/1) ash bed, sharp base, subtle normal grading into overlying ooze
T6	591	5-3, 144	36.64	1.5	early Pleist.	*1.37*[2] 1.33[2]	Distinct greenish gray (5GY 6/2) ash layer, sharp base, diffuse bioturbated top
T7	591	25A-3, 25	230.75	1	late Mio.	7.0[1]	Scattered grayish olive (10Y 4/2) ash pods formed by bioturbation
T8	592	2-6, 83	12.83	5	middle Pleist.	*0.85*[2] 0.95[2]	Distinct light gray (N6) ash bed, sharp base, irregular top and disrupted by bioturbation
T9	593	3-5, 78	21.50	10	middle Pleist.	0.93[2]	Distinct medium gray (N5) ash bed, sharp base, burrowed irregular top
T10	593	4-4, 30	29.10	<1	early Pleist.	*1.26*[2] 1.38[2]	Diffuse grayish yellow green (5GY 7/2) ash layer and wisps possibly due to bioturbation
T11	593	4-4, 80	29.60	1	early Pleist.	*1.26*[2] 1.38[2]	Diffuse grayish yellow green (5GY 7/2) ash pods and wisps formed by bioturbation
T12	593	4-4, 100	29.80	2	early Pleist.	*1.26*[2] 1.38[2]	Distinct grayish yellow green (5GY 7/2) ash layer, sharp base, disrupted by bioturbation
T13	594	5-2, 30	36.50	10	late Pleist.	0.28[1] *0.27*[2]	Diffuse, soupy-textured, massive bluish gray (5B 6/1) ash with moderately sharp contacts
T14	594	12-2, 40	103.80	2	middle Pleist.	*0.77*[2] 0.73 to 1.66[2]	Diffuse dark greenish gray (5GY 6/1) ash bed with abruptly gradational contacts with ooze
T15	594	8A-3, 50	112.00	1	middle Pleist.	*0.85*[2] 0.73 to 1.66[2]	Diffuse light olive gray (5Y 6/1) ash layer disrupted by bioturbation
T16	594	10A-6, 6	157.46	3	early Plio.	*3.9*[1] 2.2 to >2.47[2]	Distinct but partly disrupted dark gray (N3) ash bed with upward dissemination of ash
T17	594	28-5, 56	262.06	2	late Mio.	8.6[1]	Diffuse light olive gray (5Y 6/1) ash layer with sharp lower and gradational upper contact with ooze
T18	594	36, CC	341.75	7	mid Mio.	9.4[1]	Diffuse olive gray (5Y 4/1) ash bed, sharp base, gradational top

[a] Estimated age assuming constant rates of sedimentation between dated boundaries of associated nannofossil (1) or paleomagnetic (2) zones. Where two ages are given, the italicized age is preferred.
[b] PGL = pale green laminae (Gardner, Nelson, et al., this volume).

Table 2. General grain size classification and mineralogic composition[a] of megascopic tephras in Leg 90 sediments.

	T1	T2	T3	T4	T5	T6	T7	T8	T9	T10	T11	T12	T13	T14	T15	T16	T17	T18
Grain size (mm)																		
Dominant[b]	fsu	vfsu	msl	vfsl	fsl	vfsu	vfsu	fsu	fsl	vfsu	fsl	vfsu	fsl	vfsu	vfsu	fsu	fsu	vfsl
Maximum	0.4	0.4	0.8	0.2	0.3	0.3	0.3	0.3	0.3	0.2	0.3	0.2	0.3	0.2	0.2	0.3	0.3	0.2
Mineralogy																		
Magnetite			R															
Pyrite	R			C	R		T					R			R	R	R	
Altered fragments[c]		A	C	C	C		R	C	C	R	R	C	C	C	C	C	R	C
Hypersthene								R	R	T	T	T	R	T	R	R	T	
Green hornblende					T				T	T			T		R	T	T	
Brown hornblende																T		T
Biotite				C	R			R	T		T		T	R			C	R
Muscovite																		C
Plagioclase	R	R	A	T	T			T	T	T	T	T	T	T		T		
Quartz								T	T	T			T					T
Glass shards																		
Clear	A	R		C	A	A	A	A	A	A	A	A	A	A	A	A	A	C
Brown					R				R				R	R	T	T		

[a] A = abundant; C = common; R = rare; T = trace.
[b] vfsl and vfsu = very fine sand lower (0.06–0.10 mm) and upper (0.10–0.13 mm), respectively; fsl and fsu = fine sand lower (0.13–0.19 mm) and upper (0.19–0.25 mm), respectively; msl = medium sand lower (0.25–0.35 mm).
[c] Includes argillized shards, limonitized fragments, and grains with ?leucoxene coatings.

Table 3. Microprobe analysis of pyrite replacing glass shard in tephra T1, Site 586.

	T1 pyrite	
	Wt.%	Atom
Fe	47.00	1.01
S	53.28	1.99
Cu	0.03	—
Mn	—	—
Ni	0.02	—
	100.33	3.00

mineralogy typical of silicic tephras (Table 2). Thus, whereas most of the megascopic tephras (T4 to T18) in Leg 90 sediments were derived from silicic magmas, tephras T1 to T3 had a basic or intermediate magma source.

INTERCORE CORRELATION

Several of the megascopic tephra samples have a glass chemistry (Table 5) distinctive enough to be positively differentiated (Fig. 6). Some of the tephras overlap in their glass chemistry, and those of a similar age probably are correlative. None of the analyzed Miocene or Pliocene tephras (T1 to T4, T7, and T16 to T18) are sufficiently similar in composition and age (Tables 1 and 5; Fig. 6) to be regarded as correlatives so that eight separate explosive events are indicated by the Neogene megascopic tephras—three basaltic and five silicic. Of the 10 Quaternary tephras (T5, T6, and T8 to T15), samples T5 and T13 are chemically identical and of similar late Pleistocene age, samples T6 and T10 to T12 are likewise chemically similar and of comparable early Pleistocene age, and samples T8 and T9 form a third chemical cluster and are of middle Pleistocene age. Of the two remaining Quaternary tephras, both are middle Pleistocene, but T14 is chemically unique, and T15 clearly plots as two distinct clusters on Figure 6, one falling within the T6/T10/T11/T12 field and the other being unique. The cause of this bimodality is not clear and, although biologic mixing of tephras may be represented, interpretation is hampered by the uncertain paleomagnetic zones at Site 594 (see Site chapter, this volume). Thus the between-core correlation implied on the basis of age and glass chemistry indicates that the 10 Quaternary tephras analyzed record at most five eruptive events, all silicic (Fig. 7).

TEPHRA SOURCES

Since New Zealand is the only area in the southwest Pacific with voluminous silicic volcanism during the late Cenozoic (Fig. 1), it is the most likely source of the silicic ash layers in all Leg 90 cores. The Coromandel region and the Central Volcanic Region of North Island have produced large-volume silicic eruptions from middle Miocene to Pliocene and throughout the Quaternary, respectively (Fig. 1; Ballance, 1976; Suggate et al., 1978; Cole, 1979). The glass chemistry of the Leg 90 silicic tephras is compatible with the known chemistry of the volcanic products from North Island sources (Ewart, 1963, 1966; Froggatt, 1983; Gosson, in prep.).

The Leg 90 silicic tephras are still not correlated with specific source eruptions. Of several silicic tephras in

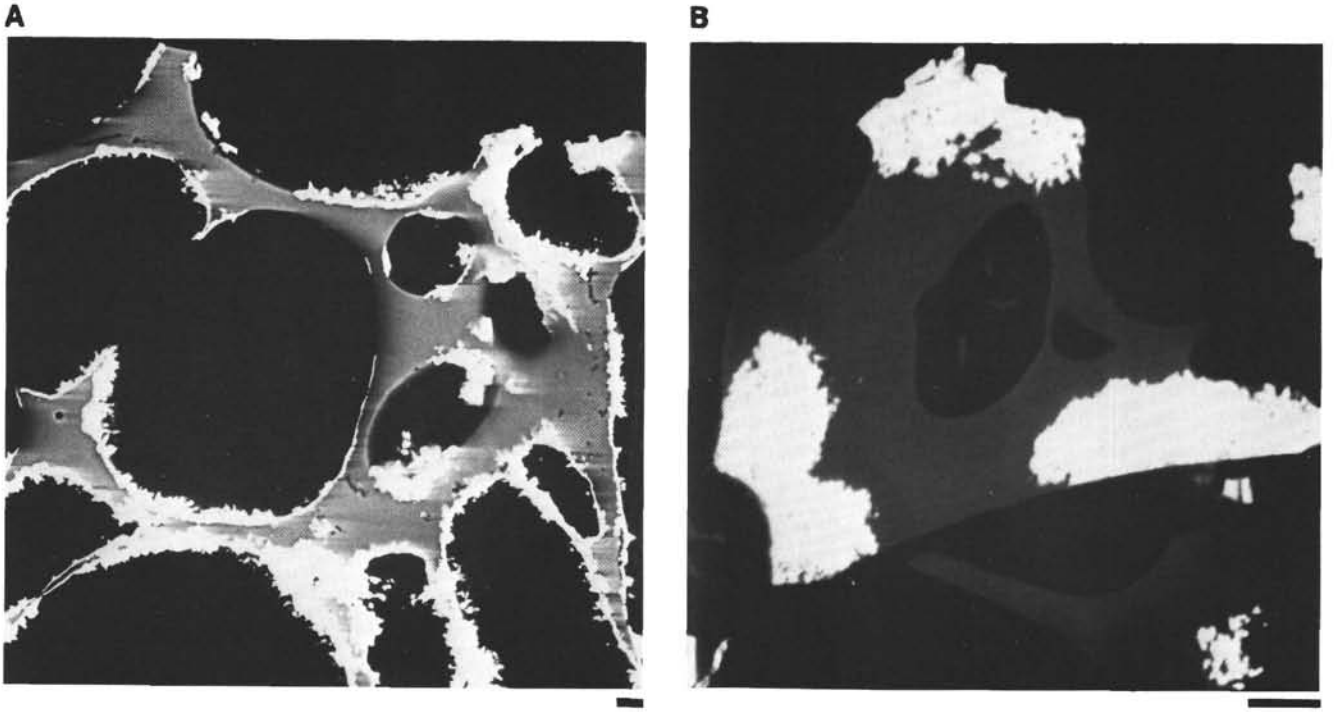

Figure 4. Back-scattered electron images of polished sections showing association of pyrite with glass shards. Bar scale 10 μm. A. Pyrite crystals (white) coating the surface of a basaltic glass shard in tephra T1, apparently without significant replacement of the glass (see also Plate 1, Fig. 1) B. Microcrystalline pyrite (white) replacing portions of silicic glass shards in tephra T4.

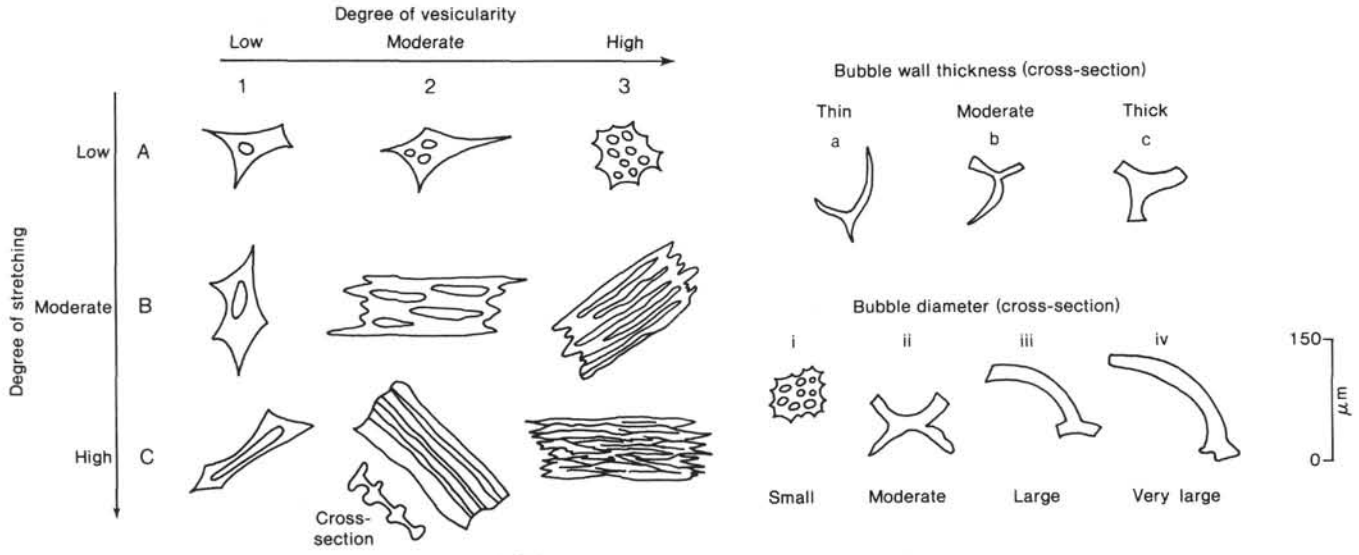

Figure 5. Descriptive terminology for morphologic classification of glass shards in the 60–250 μm size fraction (from Gosson, in prep.).

Table 4. General morphologic features of dominant glass shard types in megascopic tephras from Leg 90 cores. Categories defined in Figure 5.

	Vesicularity			Stretching			Bubble diameter				Bubble wall thickness		
Tephra	1	2	3	A	B	C	i	ii	iii	iv	a	b	c
T1		X	X	X				X			X		
T2			X	X			X	X			X		
T4	X			X				X	X			X	X
T5	X	X			X				X		X	X	
T6	X			X				X				X	X
T7	X	X		X	X			X	X			X	
T8		X			X				X			X	
T9	X	X		X	X			X	X				X
T10	X			X				X	X		X	X	
T11	X	X		X				X	X		X	X	X
T12	X	X		X				X			X		X
T13	X			X					X			X	
T14		X	X	X			X					X	X
T15	X			X						X		X	
T16		X	X	X	X		X	X			X		
T17	X			X				X	X				X
T18	X			X	X			X	X			X	X

piston cores of abyssal sediments from east of New Zealand, five, labeled A to E by Ninkovich (1968), were tentatively correlated using paleomagnetic dating (Watkins and Huang, 1977) with tephras in Pleistocene marine sediments on land (Seward, 1974, 1976). Using glass analyses, Froggatt (1983) has suggested that land equivalents of three of Ninkovich's deep-sea tephras are widespread in North Island and has related two of them to specific ignimbrites. The glasses in deep-sea tephras A and D are compositionally similar to and likely correlatives of two separate sets of equivalently aged tephras in Leg 90 cores (Fig. 7). Froggatt (1983) has correlated tephra D with the widespread Mt. Curl tephra of New Zealand, and the Whakamaru ignimbrite of the Central Volcanic Region, the source vent for which was probably Lake Taupo (Briggs, 1976). The evidence is a combination of similar stratigraphic position and a common distinctive glass chemistry, with high K_2O values (>4.00%) and a Na_2O/K_2O ratio much less than 1.0 (typically 0.8). The Leg 90 tephras T5 and T13 are chemically indistinguishable (Table 5), have similar stratigraphic position, and thus are possibly distal air-fall correlatives of Whakamaru ignimbrite. Moreover, tephras T5 and T13 are among the thickest recorded in Leg 90 cores (Table 1). Tephra T5 is located over 500 km northwest of New Zealand (Site 591), whereas tephra T13 was cored at Site 594, 250 km off eastern South Island (Fig. 1). An extremely large eruptive event is implied.

The Coromandel region of northern North Island (Ballance, 1976; Suggate et al., 1978) is probably the eruptive source of the pre-Quaternary silicic tephras in Leg 90 cores, but specific centers cannot be determined. The volcanic history of Coromandel is poorly understood, and the Neogene tephrostratigraphy there virtually is unknown. A partial record of Coromandel volcanic activity is preserved as primary and reworked tephras in thick (>7 km) marine sequences now uplifted in eastern North Island (Gosson, in prep.). Tentative correlations of Leg 90 tephras with these tephras can be made as follows. Figure 8 is a graphical means (after Sarna-Wojcicki et al., 1984) of displaying the similarities and differences between the shard chemistry of two samples. Ratios are calculated by dividing the mean weight percent of an element in a Neogene tephra sample from land by the mean weight percent of the same element in a Leg 90 tephra sample. Chemically similar samples will have ratios close to 1.00 for each element, whereas differences will be shown by ratios greater or less than 1.00. Seven eastern North Island late Miocene tephras that are closest in chemistry to tephra T17 (Table 5) are compared with tephra T17 in Figure 8A. Samples G019, G255, and G256 are most similar to tephra T17 and, being comparable in age, could be correlatives. The abundance of biotite in both tephras T17 (Table 2) and G019 (Gosson, in prep.) strengthens the suggested correlation between these two tephras. A similar approach for late Miocene tephra T7

Table 5. Chemical composition of glass shards from megascopic tephras in Leg 90 cores.

	T1	T4	T5	T6	T7	T8	T9	T10
Si_2O	51.48 (0.25)	77.40 (0.24)	77.14 (0.21)	75.26 (0.30)	77.62 (0.27)	77.82 (0.24)	77.62 (0.22)	75.63 (0.56)
Al_2O_3	14.02 (0.10)	12.55 (0.10)	12.42 (0.10)	13.26 (0.13)	12.16 (0.11)	12.24 (0.08)	12.40 (0.12)	12.99 (0.20)
TiO_2	2.35 (0.07)	0.07 (0.05)	0.16 (0.03)	0.14 (0.05)	0.18 (0.04)	0.12 (0.04)	0.12 (0.04)	0.16 (0.05)
FeO*	10.94 (0.21)	0.94 (0.19)	1.07 (0.08)	1.95 (0.12)	1.18 (0.09)	1.06 (0.12)	1.08 (0.13)	2.00 (0.19)
MgO	6.74 (0.13)	0.06 (0.04)	0.12 (0.03)	0.08 (0.01)	0.14 (0.02)	0.10 (0.03)	0.09 (0.04)	0.09 (0.02)
CaO	11.27 (0.10)	0.57 (0.21)	0.82 (0.03)	0.98 (0.05)	1.10 (0.08)	0.89 (0.12)	0.86 (0.13)	1.04 (0.12)
Na_2O	2.75 (0.06)	3.66 (0.24)	3.60 (0.13)	4.59 (0.21)	3.38 (0.11)	3.74 (0.15)	3.89 (0.11)	4.36 (0.19)
K_2O	0.32 (0.05)	4.63 (0.76)	4.46 (0.17)	3.57 (0.13)	4.05 (0.15)	3.80 (0.33)	3.73 (0.25)	3.55 (0.18)
Cl	0.13 (0.05)	0.12 (0.02)	0.23 (0.03)	0.16 (0.04)	0.19 (0.03)	0.22 (0.03)	0.22 (0.03)	0.17 (0.03)
Water[a]	2.33 (0.53)	6.14 (0.78)	5.21 (0.45)	5.79 (1.04)	6.89 (1.62)	4.96 (1.04)	5.53 (0.56)	5.38 (1.04)
N	15	14	14	13	14	15	15	15
Na/K	8.59	0.79	0.81	1.29	0.83	0.98	1.04	1.23
	T11	T12	T13	T14	T15	T16	T17	T18
SiO_2	75.41 (0.39)	75.53 (0.74)	77.06 (0.37)	74.88 (0.97)	76.25 (0.72)	76.25 (0.32)	77.41 (0.36)	77.11 (0.23)
Al_2O_3	13.20 (0.21)	12.87 (0.36)	12.47 (0.19)	13.46 (0.34)	12.58 (0.33)	13.05 (0.22)	12.79 (0.16)	12.75 (0.10)
TiO_2	0.16 (0.04)	0.15 (0.04)	0.15 (0.03)	0.22 (0.05)	0.13 (0.07)	0.17 (0.04)	0.05 (0.03)	0.07 (0.03)
FeO*	1.97 (0.10)	1.95 (0.23)	1.03 (0.09)	2.33 (0.20)	1.80 (0.28)	1.58 (0.17)	0.76 (0.11)	0.95 (0.06)
MgO	0.09 (0.03)	0.10 (0.02)	0.11 (0.03)	0.18 (0.07)	0.07 (0.02)	0.16 (0.07)	0.04 (0.03)	0.05 (0.03)
CaO	1.01 (0.09)	1.01 (0.15)	0.81 (0.04)	1.36 (0.18)	0.92 (0.15)	1.26 (0.16)	0.49 (0.14)	0.72 (0.03)
Na_2O	4.51 (0.17)	4.55 (0.21)	3.67 (0.13)	4.26 (0.33)	4.33 (0.25)	3.99 (0.28)	3.67 (0.19)	3.52 (0.19)
K_2O	3.44 (0.10)	3.65 (0.17)	4.46 (0.12)	3.12 (0.17)	3.72 (0.24)	3.39 (0.41)	4.67 (0.39)	4.67 (0.17)
Cl	0.21 (0.04)	0.20 (0.04)	0.24 (0.03)	0.19 (0.01)	0.20 (0.05)	0.16 (0.03)	0.12 (0.02)	0.16 (0.03)
Water[a]	5.60 (0.81)	5.86 (1.99)	6.14 (1.77)	6.10 (0.81)	6.31 (1.27)	6.33 (1.45)	6.86 (1.54)	6.07 (0.89)
N	15	15	12	15	15	15	14	15
Na/K	1.31	1.25	0.82	1.37	1.16	1.18	0.79	0.75

Note: * All Fe calculated as FeO. *N* = number of analyses in mean. Numbers in parentheses are 1 standard deviation.
[a] Water by difference.

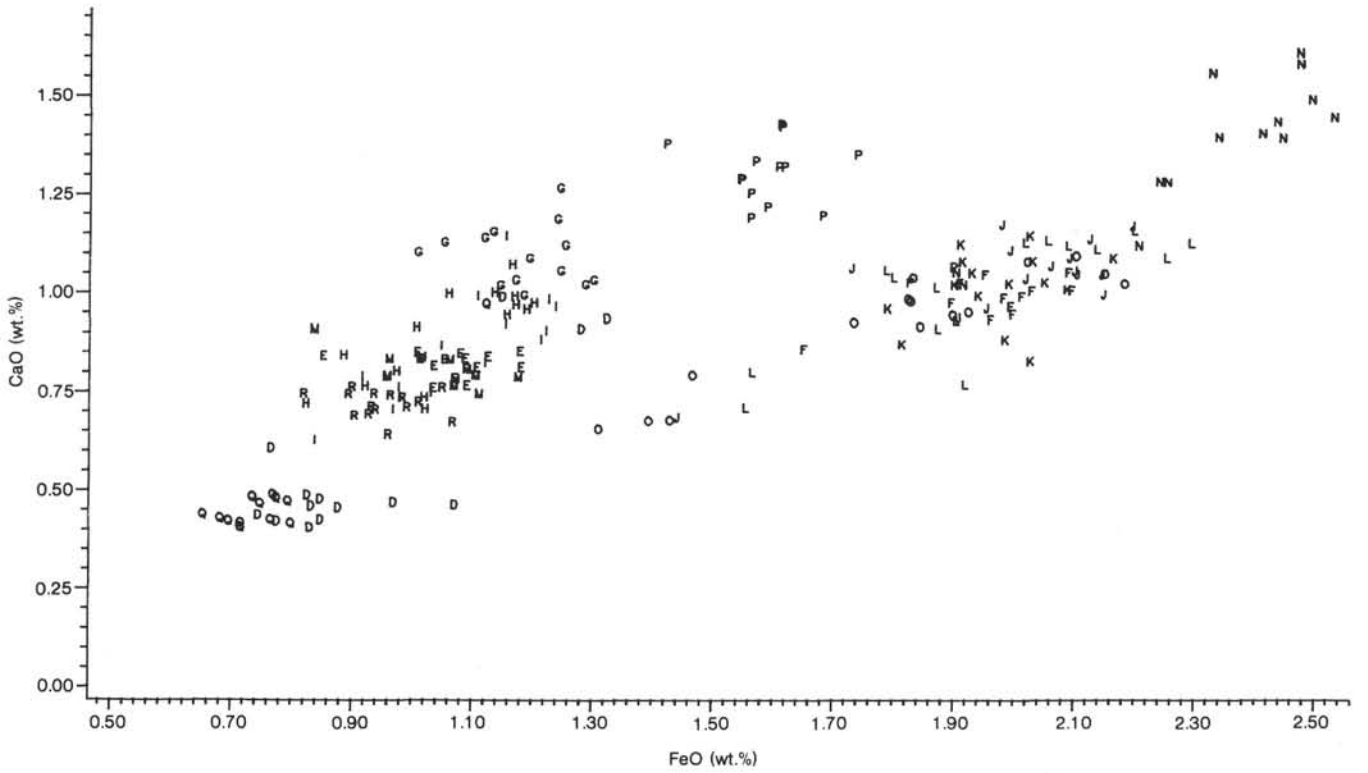

Figure 6. Plot of CaO versus FeO (Table 5) for the glass shards from 15 megascopic tephras (T4 to T18) in Leg 90 sediments. Letter symbols D through R correspond to tephras T4 through T18, respectively.

Table 6. Comparison of chemical composition of basaltic glasses from mid-ocean ridge (1,2), ocean island (3,4,5), and island arc (6) settings (from Basaltic Volcanism Study Project, 1981) with glass from tephra T1 (Site 586).

	1	2	3	4	5	6	T1
SiO_2	50.19	50.93	49.60	48.70	50.40	50.90	51.48
Al_2O_3	14.86	15.15	13.60	12.20	13.30	17.80	14.02
TiO_2	1.77	1.19	2.88	2.50	3.80	0.95	2.35
FeO*	11.33	10.32	11.00	11.40	12.20	9.50	10.94
MnO	—	—	0.10	0.10	0.10	0.19	—
MgO	7.10	7.69	6.24	9.69	5.20	6.00	6.74
CaO	11.44	11.84	11.00	10.80	9.59	10.40	11.27
Na_2O	2.66	2.32	2.37	2.05	2.74	2.73	2.75
K_2O	0.16	0.14	0.57	0.47	0.75	0.82	0.32
Cr_2O_3	—	—	0.01	0.01	—	—	—
P_2O_5	0.14	0.10	—	—	—	0.23	—
	99.65	99.68	97.37	98.01	98.08	99.52	99.87

Note: 1,2 = Average basaltic glass from East Pacific Rise and Indian Ocean spreading centers. 3,4,5 = Average composition of Hawaiian glasses HAW-21, HAW-23, HAW-25, respectively. 6 = Average composition of island arc basalts. * All Fe calculated as FeO. — = not detected.

Table 7. Representative chemical composition of plagioclase crystals from Sites 586 and 587.

	T1	T3
SiO_2	51.93	54.83
Al_2O_3	29.41	28.54
TiO_2	0.08	0.02
FeO*	0.94	0.21
MnO	0.01	0.02
MgO	0.29	0.01
CaO	14.02	11.46
Na_2O	3.65	4.93
K_2O	0.07	0.34
NiO	0.01	0.01
Cr_2O_3	0.03	
	100.44	100.37
Number of ions based on 8(0)		
Si	2.362	2.469
Al	1.577	1.515
Ti	0.003	0.001
Fe*	0.035	0.008
Mn	—	0.001
Mg	0.020	0.001
Ca	0.683	0.553
Na	0.322	0.431
K	0.004	0.020
	5.006	4.999
Ab	31.9	42.9
An	67.7	55.1
Or	0.4	2.0
N	4	4

Note: * All Fe calculated as ferrous. *N* = number of analyses in mean. — = not considered.

(Fig. 8B) indicates chemical similarity and possible correlation with tephra G052, an eastern North Island tephra with an estimated age between 7 and 7.5 m.y.

Surface winds from between the northwest and southwest prevail over New Zealand (Fig. 9) so that volcanic ash from North Island should be transported to the east

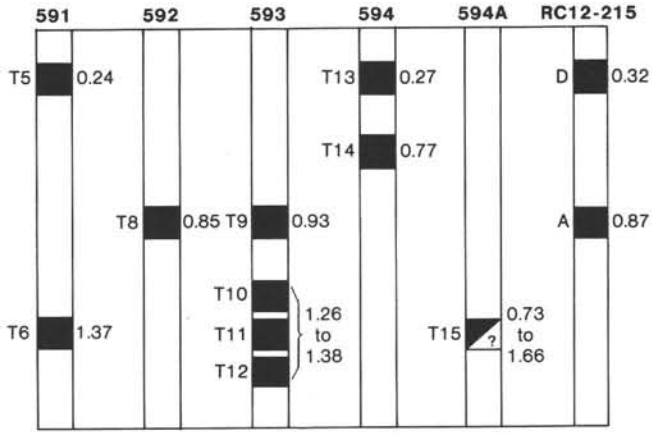

Figure 7. Schematic diagram illustrating possible correlation of Quaternary megascopic tephras in Leg 90 cores with each other and with the deep-sea tephras A and D described from core RC12-215 off eastern New Zealand by Ninkovich (1968) and Watkins and Huang (1977). Estimated ages (m.y.) of tephras (Table 1) shown to right of each column.

of New Zealand. Dispersal in this anticipated direction was confirmed by Ninkovich (1968) and Watkins and Huang (1977). Here we have documented the occurrence of North Island–derived Neogene and Quaternary megascopic silicic tephras west and northwest of New Zealand at Sites 590 through 593 in the Tasman Sea. Moreover, disseminated silicic shards of a probable New Zealand origin occur in the Lord Howe Rise oozes at least as far north as Site 588 (Site chapter, this volume). Possible explanations for the transport of ash from New Zealand into the central and northern Tasman Sea include: (a) eruption at a time when upper-level winds were blowing from the east which, at the present day, occurs up to 5 to 20% of the time over northern New Zealand, the frequency varying with altitude (Table 8); (b) dispersal of ash first east and northeast of North Island by the prevailing westerlies (Fig. 9; Reid, 1982) and then west and northwest into the Tasman Sea, either because of the natural anticyclonic curvature of surface winds in the region (Ramage, 1970; Steiner, 1980) or because the ash enters into the belt of southeasterly through easterly trade winds off northern New Zealand (Fig. 9); and (c) direct northwestward transport by stratospheric (south)easterly winds which, at the present day, prevail above 20 km altitude between September and March over New Zealand (J. W. D. Hessell, New Zealand Meteorological Service, pers. comm., 1984). This last option can account for the opposing directions of ash dispersal implied, for example, by correlating tephra T5 with tephra T13 and D, and tephras T8 and T9 with tephra A (cf. Figs. 1 and 7), the ash below and above about 20 km altitude being "simultaneously" dispersed in opposite directions toward the Pacific Ocean and Tasman Sea, respectively.

The source regions of the nonsilicic tephras T1 to T3 are less readily identified. Tephra T1 (Site 586) has a glass chemistry typical of an ocean island source (Table 6), which abound in the vicinity of the Ontong-Java Plateau. Tephras T2 (Site 587) and T3 (Site 588) also are basic or intermediate (see earlier) and are derived from

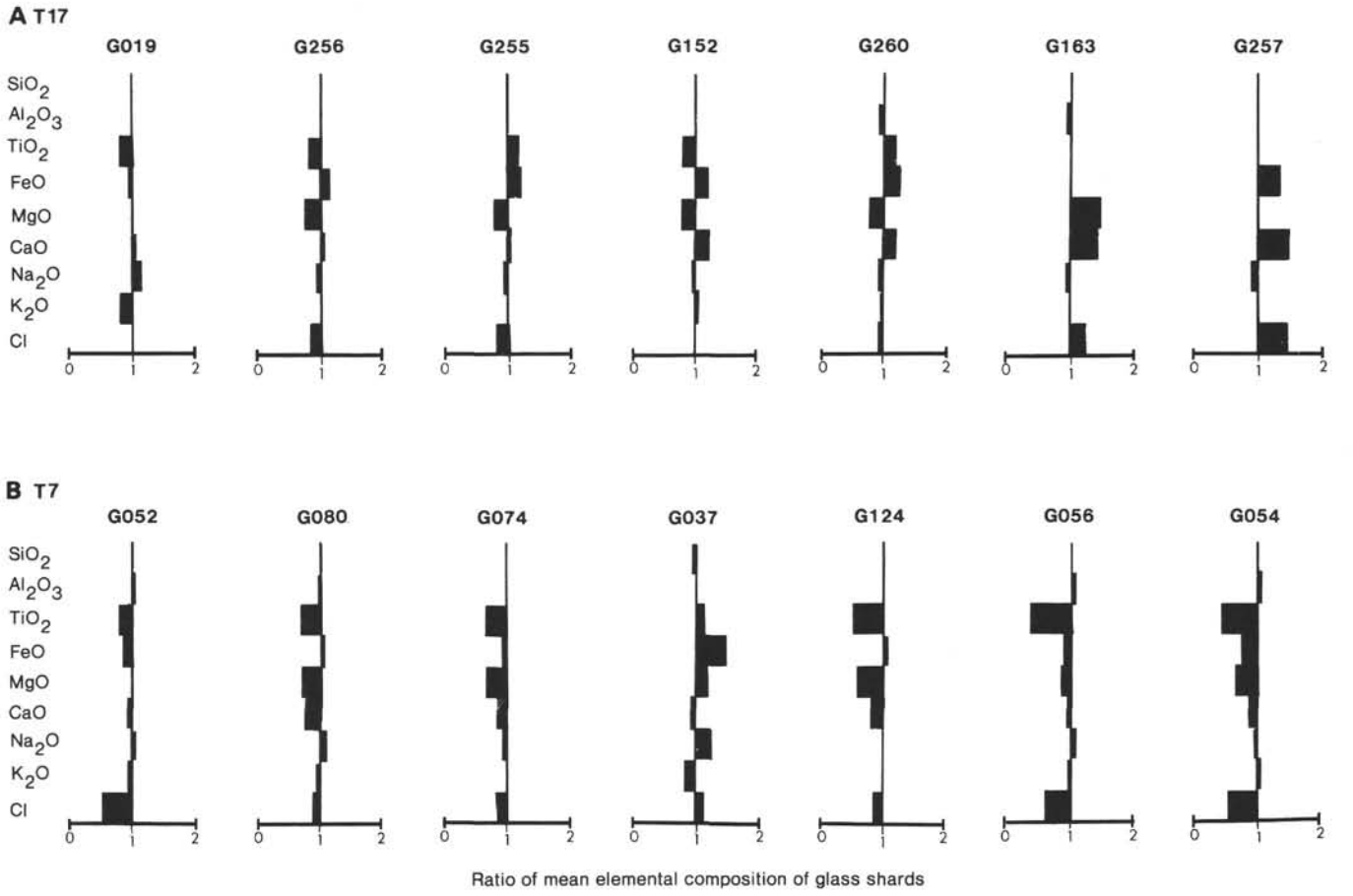

Figure 8. Comparison of elemental composition (as ratio of means) of glass shards from late Miocene deep-sea tephras T17 (A) and T7 (B) with several equivalently aged tephras from New Zealand as a possible way of determining correlative eruptive events. Tephra chemistry for land samples (labeled G) from Gosson (in prep.). Chemical affinity is indicated where the ratios are very close to 1.00 for each element. See text for discussion.

ocean ridge or ocean island volcanoes. Churkin and Packham (1973) suggested that prevailing wind and ocean current directions in the northern South Fiji Basin are both toward the southwest so that a source from Vanuatu (New Hebrides) arc is favored (Fig. 1). Tephras T1 to T3 are each generally coarser than the silicic ashes (Table 2), suggesting closer volcanic sources.

CONCLUSIONS

Eighteen late Cenozoic megascopic vitric tephras are described from Leg 90 sediments in the Tasman Sea and off eastern South Island, New Zealand. Fifteen of these are silicic, derived from eruptions in North Island, New Zealand. Several of the Quaternary silicic tephras are correlatives, and at least two are matched to the on-land Mt. Curl tephra (~0.25 m.y.), possibly associated with eruption of Whakamaru ignimbrite from Lake Taupo, North Island. The occurrence of North Island–derived tephras in Tasman Sea sediments suggests that ash transported eastward by the prevailing westerly airstream across New Zealand may be diverted northwest and west on entering the southeasterly trade wind belt off northeastern New Zealand. In the case of large eruptions, ash ascending above 20 km altitude may be carried directly toward the Tasman Sea by easterly stratospheric winds, while coeval lower-level ash drifts east of New Zealand into the southern Pacific Ocean.

The three analyzed nonsilicic megascopic tephras comprise altered basic shards and common labradorite crystals derived from ocean island or ridge explosive volcanism in the Ontong-Java Plateau and Vanuatu regions.

The megascopic tephras are a fragmentary record of late Cenozoic volcanism in the southwest Pacific since New Zealand–derived silicic shards are a ubiquitous but disseminated minor component in many of the sediments. More importantly, innumerable thin bentonite layers occur in Leg 90 cores, probably representing devitrified intermediate to basic tephras derived mainly from oceanic arc volcanism at the Pacific/Australian plate boundary (Gardner, Nelson, et al., this volume). In contrast to the silicic shards, the preservation potential of more basic shards was low in the calcareous sediments.

ACKNOWLEDGMENTS

We thank Professor Paul Vella (Department of Geology, Victoria University, Wellington) and Dr. William G. Melson (Smithsonian Institution) for their reviews of this paper.

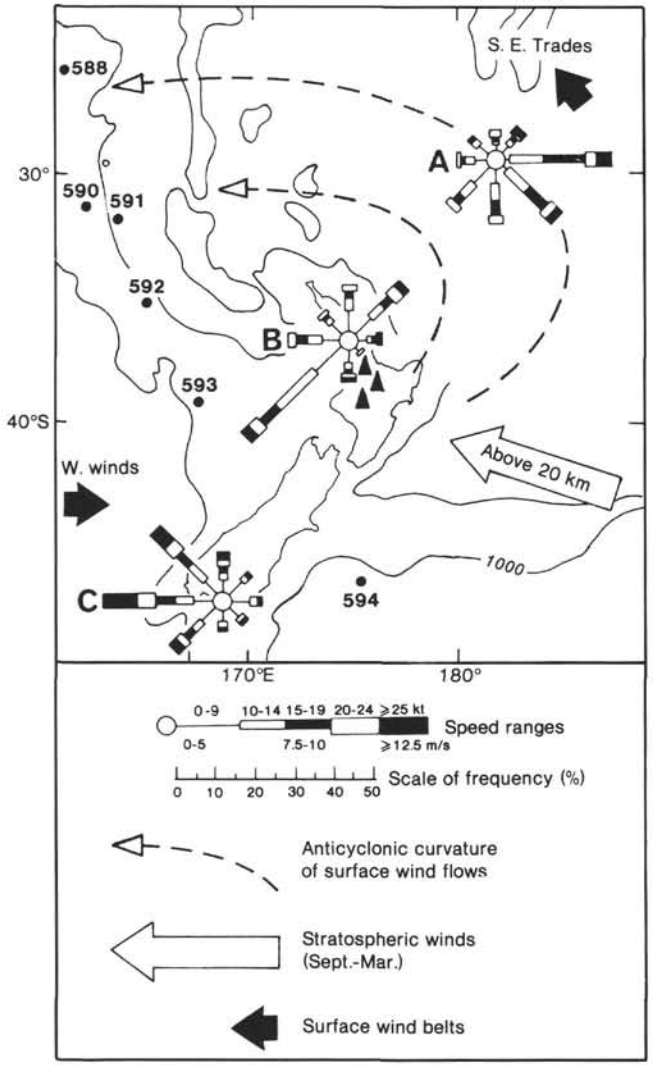

Figure 9. Some present-day wind characteristics in the New Zealand sector of the southwest Pacific. Open-ocean surface wind frequency diagrams for upper wind stations A, B, and C for Raoul Island, Auckland, and Invercargill, respectively, are from Reid (1982). See text for discussion.

Table 8. Some upper-level wind frequencies and mean speeds measured above Auckland over the period 1966–1979 (data from Reid and Penney, 1982).

mb	Altitude (km)	Mean wind speed (mps)	% time wind occurs from SE	E	NE
100	16	15	1.2	0.6	0.5
200	12	28	1.7	0.6	0.6
300	9	24	3.4	1.8	2.0
500	6	15	4.7	2.9	3.3
700	3	11	6.3	5.3	5.6
900	1	9	5.8	8.0	10.2

REFERENCES

Ballance, P. F., 1976. Evolution of the Upper Cenozoic magmatic arc and plate boundary in northern New Zealand. *Earth Planet. Sci. Lett.*, 28:356–370.

Basaltic Volcanism Study Project, 1981. *Basaltic Volcanism on the Terrestrial Planets:* New York (Pergamon Press, Inc.).

Briggs, N. D., 1976. Welding and crystallization zonation in Whakamaru Ignimbrite, central North Island, New Zealand. *N.Z. J. Geol. Geophys.*, 19:189–212.

Burns, R. E., Andrews, J. E., et al., 1973. *Init. Repts. DSDP*, 21: Washington (U.S. Govt. Printing Office).

Churkin, M., and Packham, G. H., 1973. Volcanic rocks and volcanic constituents in sediments, Leg 21, Deep Sea Drilling Project. *In* Burns, R. E., Andrews, J. E., et al., *Init. Repts. DSDP*, 21: Washington (U.S. Govt. Printing Office), 481–493.

Cole, J. W., 1979. Structure, petrology, and genesis of Cenozoic volcanism, Taupo Volcanic Zone, New Zealand—a review. *N.Z. J. Geol. Geophys.*, 22:631–657.

Ewart, A., 1963. Petrology and petrogenesis of the Quaternary pumice ash in the Taupo area, New Zealand. *J. Petrol.*, 4:392–431.

_____, 1966. Review of mineralogy and chemistry of the acidic rocks of Taupo Volcanic Zone, New Zealand. *Bull. Volcanol.*, 29: 147–172.

Ewart, A., Hildreth, W., and Carmichael, I. S. E., 1975. Quaternary acid magma in New Zealand. *Contrib. Mineral. Petrol.*, 51:1–27.

Froggatt, P. C., 1983. Toward a comprehensive Upper Quaternary tephra and ignimbrite stratigraphy in New Zealand using electron microprobe analysis of glass shards. *Quat. Res.*, 19:188–200.

Kennett, J. P., 1981. Marine tephrochronology. *In* Emiliani, C. (Ed.), *The Sea* (Vol. 7): New York (John Wiley), 1373–1436.

Kennett, J. P., Houtz, R. E., et al., 1975. *Init. Repts. DSDP*, 29: Washington (U.S. Govt. Printing Office).

Kohn, B. P., 1973. Some studies of New Zealand Quaternary pyroclastic rocks [Ph.D. dissert.]. Victoria University, Wellington.

Ninkovich, D., 1968. Pleistocene volcanic eruptions in New Zealand recorded in deep sea sediments. *Earth Planet. Sci. Lett.*, 4:89–102.

Ramage, C. S., 1970. Meteorology of the South Pacific tropical and middle latitudes. *In* Wooster, W. S., (Ed.), *Scientific Exploration of the South Pacific:* Washington (National Academy of Sciences), pp. 16–29.

Reid, S. J., 1982. Surface wind frequencies in the southwest Pacific estimated from radar-wind data. *N.Z. J. Sci.*, 25:303–311.

Reid, S. J., and Penney, A. C., 1982. Upper-level wind frequencies and mean speeds for New Zealand and Pacific Island stations. *N.Z. Met. Serv. Misc. Publ.*, 174.

Sarna-Wojcicki, A. M., Bowman, H. R., Meyer, C. E., Russell, P. C., Woodward, M. J., McCoy, G., Rowe, J. J., Jr., Baedecker, P. A., Asaro, F., and Michael, H., 1984. Chemical analyses, correlations, and ages of upper Pliocene and Pleistocene ash layers of east-central and southern California. *U.S. Geol. Surv. Prof. Paper*, 1293.

Seward, D., 1974. Age of New Zealand Pleistocene substages by fission track dating of glass shards from tephra horizons. *Earth Planet. Sci. Lett.*, 24:242–248.

_____, 1976. Tephrostratigraphy of the marine sediments of the Wanganui Basin, New Zealand. *N.Z. J. Geol, Geophys.*, 19:9–20.

Steiner, J. T., 1980. The climate of the South-West Pacific region. *N.Z. Met. Serv. Misc. Publ.*, 166.

Suggate, R. P., Stevens, G. R., and Te Punga, M. T. (Eds.), 1978. *The Geology of New Zealand* (Vol. 2): Wellington (Govt. Printer).

Watkins, N. D., and Huang, T. C., 1977. Tephras in abyssal sediments east of the North Island, New Zealand: chronology, paleowind velocity, and paleoexplosivity. *N.Z. J. Geol. Geophys.*, 20:179–198.

Date of Initial Receipt: 25 June 1984
Date of Acceptance: 31 October 1984

APPENDIX

Listed here are the 54 samples originally obtained from supposedly megascopic vitric tephra layers in the course of shipboard sampling. Subsequent laboratory analyses indicated that only 18 of these samples had sufficiently abundant glass undisputedly to represent primary airfall tephras, and only these are the subject of this study. Many of the remaining samples may represent argillized ash layers (Gardner, Nelson, et al., this volume). The relative abundance of mainly fresh glass shards in the samples is shown by the letter (A, abundant; C, common; T, trace; O, absent) in parentheses next to each sample.

Site 586

11B-11, 114 cm (A)

Site 587

5-5, 49 cm (C)

Site 588

19-5, 63 cm (O)
21-2, 10 cm (O)
23-2, 145 cm (O)
3B-5, 77 cm (O)
3B-5, 83 cm (O)
3B-6, 56 cm (O)
3C-3, 74 cm (O)
6C-3, 52 cm (T)
6C-3, 149 cm (T)
12C-5, 100 cm (O)

Site 590

1-4, 71 cm (O)
4B-3, 112 cm (O)
5B-2, 82 cm (O)
5B-5, 66 cm (T)
38B-4, 113 cm (C)

Site 591

2-2, 54 cm (A)
3-2, 80 cm (O)
3-4, 48 cm (O)
3-4, 80 cm (O)
5-3, 144 cm (C)
13-6, 49 cm (T)
1A-3, 62 cm (O)
25A-3, 25 cm (C)

Site 592

2-6, 83 cm (A)
21-6, 12 cm (O)
33-5, 77 cm (T)
34-4, 143 cm (T)

Site 593

3-2, 96 cm (O)
3-5, 80 cm (A)
4-1, 80 cm (T)
4-2, 80 cm (T)
4-4, 30 cm (C)
4-4, 80 cm (C)
4-4, 100 cm (C)
25-6, 122 cm (O)
25,CC (O)
26-6, 30 cm (T)
29-5, 105 cm (O)
32-4, 118 cm (O)
33-4, 2 cm (T)
47-5, 39 cm (O)

Site 594

5-2, 33 cm (A)
12-2, 40 cm (A)
13,CC (O)
15-5, 15 cm (O)
15-5, 20 cm (O)
20-4, 19 cm (O)
28-5, 57 cm (A)
36,CC (A)
51-1, 105 cm (O)
8A-3, 50 cm (A)
10A-6, 6 cm (A)

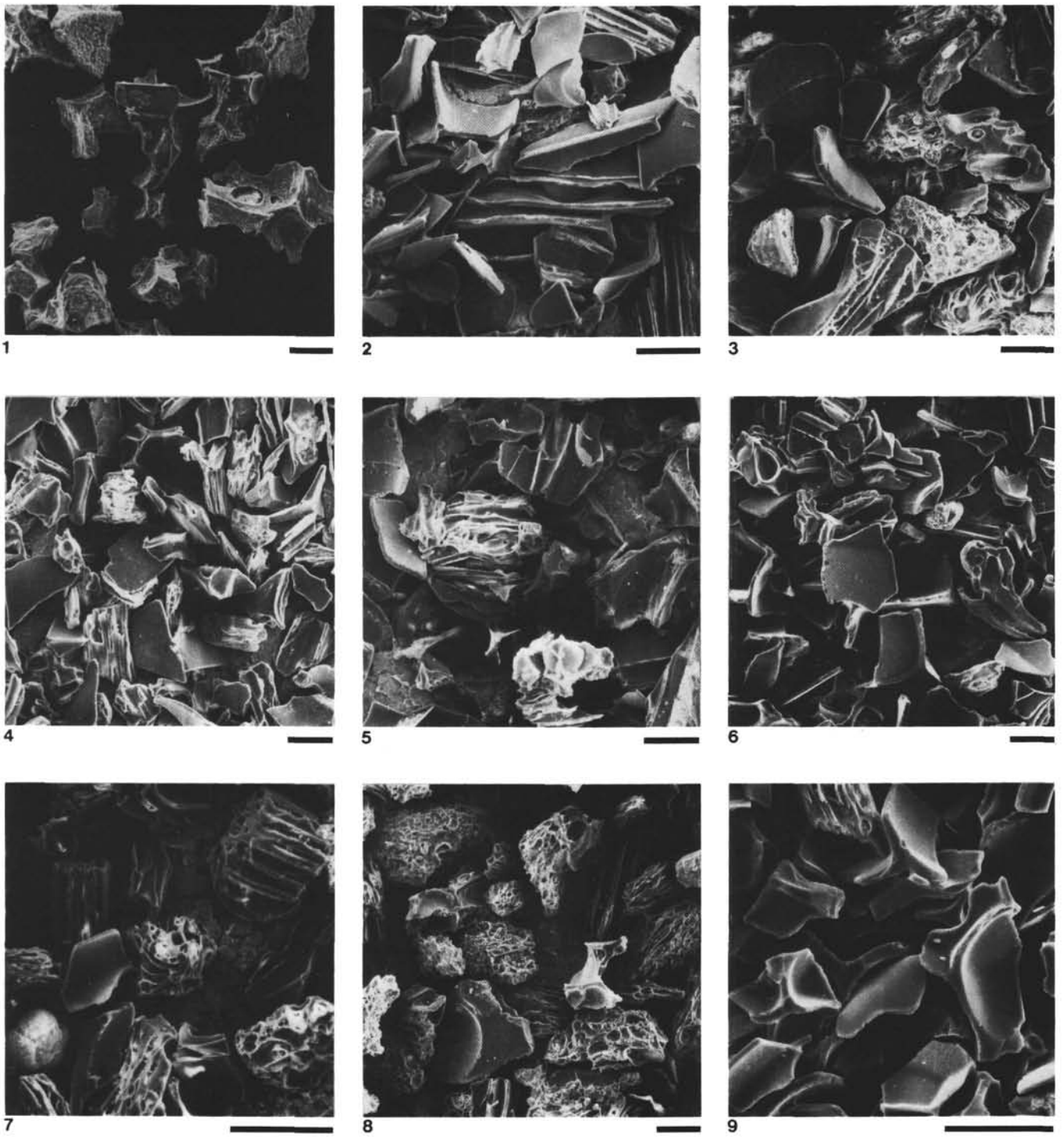

Plate 1. Scanning electron micrographs of glass shards from several megascopic tephras in Leg 90 cores. Dominant morphologic features are summarized in Table 4. Bar scale is 100 μm. Tephras are as follows: **1.** T1, 586B-11-3, 114 cm. **2.** T5, 591-2-2, 54 cm. **3.** T8, 592-2-6, 83 cm. **4.** T9, 593-3-5, 80 cm. **5.** T11, 593-4-4, 80 cm. **6.** T13, 594-5-2, 33 cm. **7.** T14, 594-12-2, 40 cm. **8.** T16, 594A-10-6, 6 cm. **9.** T18, 594-36,CC.